Quasi-classical trajectory study of collision energy effect on the stereodynamics of H + BrO → O + HBr reaction*

Xie Ting-Xian(解廷献)[a], Zhang Ying-Ying(张莹莹)[b], Shi Ying(石 英)[b]†, Li Ze-Rui(李泽瑞)[b], and Jin Ming-Xing(金明星)[b]

[a] *Department of Physics, Dalian Jiaotong University, Dalian* 116028, *China*
[b] *Institute of Atomic and Molecular Physics, Jilin University, Changchun* 130012, *China*

(Received 18 January 2014; revised manuscript received 6 Mrch 2014; published online 20 February 2015)

Quasi-classical trajectory (QCT) studies on the stereodynamics of H + BrO → O + HBr reaction have been performed on the X^1A' state of *ab initio* potential energy surface by Peterson [Peterson K A 2000 *J. Chem. Phys.* **113** 4598] in a collision energy range from 0 kcal/mol to 6 kcal/mol. Two of the polarization-dependent generalized differential cross sections (PDDCSs), $(2\pi/\sigma)(\mathrm{d}\sigma_{00}/\mathrm{d}\omega_t)$ (PDDCS_{00}) and $(2\pi/\sigma)(\mathrm{d}\sigma_{20}/\mathrm{d}\omega_t)$ (PDDCS_{20}) are considered. The rotational polarizations of these products show sensitive behaviors to the calculated collision energy range. Furthermore, in order to gain more knowledge about vector correlations, the product angular distribution, $P(\theta_r)$, and the dihedral angle, $P(\phi_r)$, are calculated, and the results indicate that both the rotational alignment and orientation of the product are enhanced as collision energy increases.

Keywords: quasi-classical trajectory, stereodynamics, polarization-dependent generalized differential cross sections

PACS: 34.50.Lf, 82.20.Fd, 82.20.Kh **DOI:** 10.1088/1674-1056/24/4/043402

1. Introduction

As catalytic cycle reaction of bromine-containing compounds plays a leading role in destructing the ozone, reactions of oxygen with bromides have been widely studied in recent decades.[1–5] The O + HBr → OH + Br reaction which is considered to be a prototype of the reaction between oxygen and bromides has been investigated both experimentally and theoretically. For experimental aspects, employing the crossed molecular beams accompanied by mass spectrometric detection, Balucani *et al.*[6] have found that the yield of product BrO is about 0.14±0.06. The rate constant and product yield of O + HBr → OH + Br reaction have been determined by Wine *et al.*[7] in a temperature range of 0 K–297 K. In 1990, McRae and Cohen[8] performed a high-resolution investigation of v_2 band of HOBr centered at 1162 cm^{-1}. Later in 2003, by using a high-resolution Fourier-transform absorption spectroscopy, Orphal *et al.*[9] reported the v_3 bands of HOBr near 16 μm with rotational assignments for more than 800 lines. Brouard and Valance[10] have reported the gas-phase UV/visible absorption spectrum which shows a slower photolysis rate of HOBr than previous results.

In the theoretical area, in 2000, a new accurate ground state *ab initio* potential energy surface was investigated by Peterson,[11] and the result is comparable to the previous experimental data. Using the quantum scattering method, Tang *et al.*[12] have studied the reaction probability, cross section, and the thermal rate constant of O + HBr → OH + Br reaction. Later, a three-dimensional (3D) time-dependent wave packet method[13] is used to study the ro-vibrational effect on the scalar properties of the reaction which has gained a sensitive result. Recently, we have reported a vibrational effect on the stereodynamics of the O + HBr → OH + Br reaction, which has indicated a vibrational dependency.[14] Moreover, reactions of hydrogen with halogen oxide, which are the reverse reactions of oxygen with halogen-containing species, have been investigated by using various theoretical methods in recent years.[15–17] The collision energy effects have been studied by using the QCT method to calculate the reaction probability, integral cross section, and vector properties of H + OCl → OH + Cl reaction.[18] Influences of the collision energy and the isotope on reaction H + FO → O + HF have been examined by Han *et al.*[19]

As for the calculation methods, in recent years, the quasi-classical trajectory method has been widely used to investigate the stereodynamics of chemical reactions especially for those atom–diatomic reactions.[20–26] Thus far, quite a lot of studies of the O + HBr → OH + Br reaction have been conducted. However, there has been reported neither experimental nor theoretical investigation of its reverse reaction H + BrO → O + HBr to date.

In this paper, the influence of the collision energy on the stereodynamics of H + BrO → O + HBr is presented by using the QCT method which has been further developed by Wang *et*

*Project supported by the Science Fund from Jilin University, China (Grant No. 419080106440), the Chinese National Fusion Project for ITER (Grant No. 2010GB104003), and the National Natural Science Foundation of China (Grant No. 10974069).

†Corresponding author. E-mail: shi_ying@jlu.edu.cn

© 2015 Chinese Physical Society and IOP Publishing Ltd

al.[27] and Chen *et al.*[28] The angular distributions $P(\theta_r)$ and $P(\phi_r)$, the $PDDCS_{00}$ and $PDDCS_{20}$ are also calculated and discussed.

2. Theory

2.1. Product rotational polarization and polarization-dependent generalized differential cross sections

The centre-of-mass (CM) frame is adopted in our paper and depicted in Fig. 1.[29–32] In the CM frame, the z axis is parallel to $\boldsymbol{k}$ which represents the reagent initial relative velocity vector. The y axis is perpendicular to the xz scattering plane which contains $\boldsymbol{k}$ and $\boldsymbol{k}'$ (initial and final velocity vectors). The θ_t is the angle between $\boldsymbol{k}$ and $\boldsymbol{k}'$, defined as $\cos\theta_t = (k\cdot k')/(|k|\cdot|k'|)$, which is the so-called scattering angle. The θ_r is the polar angle which is also the angle between $\boldsymbol{k}$ and the rotational angular momentum vector $\boldsymbol{j}'$ and ϕ_r is the azimuth angle and the dihedral angle of the $\boldsymbol{k}$–$\boldsymbol{k}'$–$\boldsymbol{j}'$ correlation as well. The fully correlated CM angular distribution is written as the following equation:[33–38]

$$P(\omega_t,\omega_r) = \sum_{kq}\frac{[k]}{4\pi}\frac{1}{\sigma}\frac{d\sigma_{kq}}{d\omega_t}C_{kq}(\theta_r,\phi_r)^*. \quad (1)$$

Here, $[k]=2k+1$, the $(1/\sigma)(d\sigma_{kq\pm}/d\omega_t)$ is the polarization-dependent generalized differential cross section (PDDCS) which is given by

$$\frac{1}{\sigma}\frac{d\sigma_{kq\pm}}{d\omega_t} = \sum_{k1}\frac{[k_1]}{4\pi}S^{k1}_{kq\pm}C_{k1-q}(\theta_T,0), \quad (2)$$

where

$$S^{k1}_{kq\pm} = \langle c_{k1q}(\theta_t,0)c_{kq}(\theta_r,0)[(-1)^q e^{iq\phi_r} \pm e^{-iq\phi_r}]\rangle. \quad (3)$$

The PDDCSs with $q=0$ is given as

$$\frac{1}{\sigma}\frac{d\sigma_{00}}{d\omega_t} = \frac{1}{4\pi}\sum_{k_1}[k_1]S^{k_1}_{k_0}P_{k_1}(\cos\theta_t), \quad (4)$$

$$S^{k_1}_{k_0} = \langle P_{k_1}(\cos\theta_t)P_k(\cos\theta_t)\rangle. \quad (5)$$

In our work, the two polarization-dependent generalized differential cross sections (PDDCSs), $(2\pi/\sigma)(d\sigma_{00}/d\omega_t)$ and $(2\pi/\sigma)(d\sigma_{20}/d\omega_t)$ are computed.

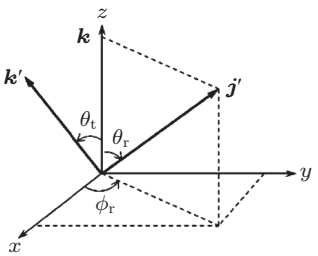


Fig. 1. Centre-of-mass coordinate system used to describe $\boldsymbol{k}$, $\boldsymbol{k}'$, and $\boldsymbol{j}'$ correlations.

The angular distribution function $P(\theta_r)$ can be expanded via the Legendre polynomials, the $P(\phi_r)$ can be expanded in Fourier series, and the joint probability density function $P(\theta_r,\phi_r)$ can be written as[35–41]

$$P(\theta_r) = \frac{1}{2}\sum_k [k]a^k_0 P_k(\cos\theta_r), \quad (6)$$

where

$$a^k_0 = \int_0^\pi P(\theta_r)P_k(\cos\theta_r)\sin\theta_r d\theta_r = \langle P_k(\cos\theta_r)\rangle, \quad (7)$$

while $k=2$ indicates the product rotational alignment, P_2 is the second Legendre moment and the brackets represent an average over the distribution of $\boldsymbol{j}'$ about k.

$$a^2_0 = \langle P_2(\cos\theta_r)\rangle = \langle P_2(j'\cdot k)\rangle = \frac{1}{2}\langle 3\cos^2\theta_r - 1\rangle, \quad (8)$$

$$P(\phi_r) = 1/2\pi\left(1 + \sum_{n_{even}\geq 2} a_n\cos n\phi_r + \sum_{n_{odd}\geq 1} b_n\sin n\phi_r\right), \quad (9)$$

where

$$a_n = 2\langle\cos n\phi_r\rangle, \quad b_n = 2\langle\sin n\phi_r\rangle, \quad (10)$$

$$\begin{aligned} P(\theta_r,\phi_r) &= \frac{1}{4\pi}\sum_{kq}[k]a^k_q C_{kq}(\theta_r,\phi_r)^* \\ &= \frac{1}{4\pi}\sum_k\sum_{q\geq 0}\left[a^k_{a\pm}\cos q\phi_r - a^k_{q\mp} i\sin q\phi_r\right]C_{kq}(\theta_r,0), \end{aligned} \quad (11)$$

where

$$a^k_q = \begin{cases} 2\langle C_{K|q|}(\theta_r,0)\cos q\phi_r\rangle, & (k=\text{even}), \\ 2\langle C_{K|q|}(\theta_r,0)\sin q\phi_r\rangle, & (k=\text{odd}). \end{cases} \quad (12)$$

In our work, the $P(\theta_r,\phi_r)$ is expanded to $k=7$ to ensure the convergence of the results.

2.2. The PES and QCT calculations

The potential energy surface (PES) in our present work is the ground state *ab initio* potential energy surface given by Peterson.[11] The multireference configuration interaction (MRCI) wave functions and basis sets of cc-pVDZ, cc-pVTZ, and cc-pVQZ are employed in the construction of the PES. It is worth emphasizing that there is deep potential well in the PES which may lead to a long-lifetime intermediate complex. A many-body expansion was employed in the analytical fitting written as:

$$\begin{aligned} V_{HOBr}(R_1,R_2,R_3) &= V^{(1)}_{OH}(R_1) + V^{(2)}_{HBr}(R_2) + V^{(2)}_{BrO}(R_3) \\ &\quad + V^{(3)}_{HOBr}(R_1,R_2,R_3), \end{aligned} \quad (13)$$

where R_1, R_2, R_3 are the OH, HBr, and BrO separate distances, respectively. The $V^{(1)}_{OH}(R_1)$ is for one-body term, the

$V^{(2)}_{\mathrm{HBr}}(R_2)$ and $V^{(2)}_{\mathrm{BrO}}(R_3)$ are for the two-body term, and the $V^{(3)}_{\mathrm{HOBr}}(R_1,R_2,R_3)$ is for three-body term.

In this work, the QCT calculation details are described below. The collision energy is chosen to be in a range of 0 kcal/mol–6 kcal/mol accompanied by running batches of 10^5 trajectories. The initial vibrational and rotational states are taken to be $v=0$ and $j=0$, respectively. An H–BrO internuclear separation is chosen to be 10 Å and an integration step size of 0.1 fs is used to assure the conservation of total angular momentum and total energy.

3. Results and discussion

Due to the demand for a multiple perspectives observation, the stereodynamical results computed in our present work are all plotted in three dimensions. The polarization-dependent differential cross sections describe the $\boldsymbol{k}$–$\boldsymbol{k}'$–$\boldsymbol{j}'$ correlation and the scattering direction of the HBr product molecule. In this paper, the $(2\pi/\sigma)(\mathrm{d}\sigma_{00}/\mathrm{d}\omega_t)$ (PDDCS_{00}) and $(2\pi/\sigma)(\mathrm{d}\sigma_{20}/\mathrm{d}\omega_t)$ (PDDCS_{20}) are computed each as a function of scattering angle and collision energy for $\mathrm{H+BrO\rightarrow O+HBr}$ reaction in a collision energy range of 0 kcal/mol–6kcal/mol. The PDDCS_{00} is a simple DCS which describes only the $\boldsymbol{k}$–$\boldsymbol{k}'$ correlation or the scattering direction of the product and has no contact with $\boldsymbol{j}'$, which is depicted in Fig. 2(a). It is seen that with increasing the collision energy, it indicates a strongly forward and backward scattering though it is a weakly sideward scattering. Furthermore, the overall trend of the forward and backward scattering shows a rising behavior, which reveals the increase of the lifetime of the intermediate complex formed in the potential well. The PDDCS_{20} is associated with the expectation value of the second Legendre moment $\langle \mathrm{P}_2(j'\cdot k)\rangle$. Obviously, the PDDCS_{20} demonstrates an opposite trend to the distribution of PDDCS_{00} which implies that $\boldsymbol{j}'$ is aligned and perpendicular to $\boldsymbol{k}$ and the values of the distributions are almost negative. Meanwhile, the behaviors of the two PDDCSs also reflect the fact that the rotational alignment of the product becomes stronger as collision energy increases.

Distributions of the product angular $P(\theta_r)$ which represents the $\boldsymbol{k}$–$\boldsymbol{j}'$ correlation are displayed in Fig. 3. We can see that all peaks of $P(\theta_r)$ are situated at $\theta_r=90^\circ$ and shows a symmetrical distribution here which implies that the rotational angular momentum vector $\boldsymbol{j}'$ is more favored to align strongly along the direction perpendicular to the direction of $\boldsymbol{k}$. Meanwhile, with increasing the collision energy, the peaks become broader and values first increase and then show a series of small variations, indicating that the product alignment becomes weaker, which is consistent with the product alignment parameter $\langle \mathrm{P}_2(j'\cdot k)\rangle$ displayed in Fig. 4.

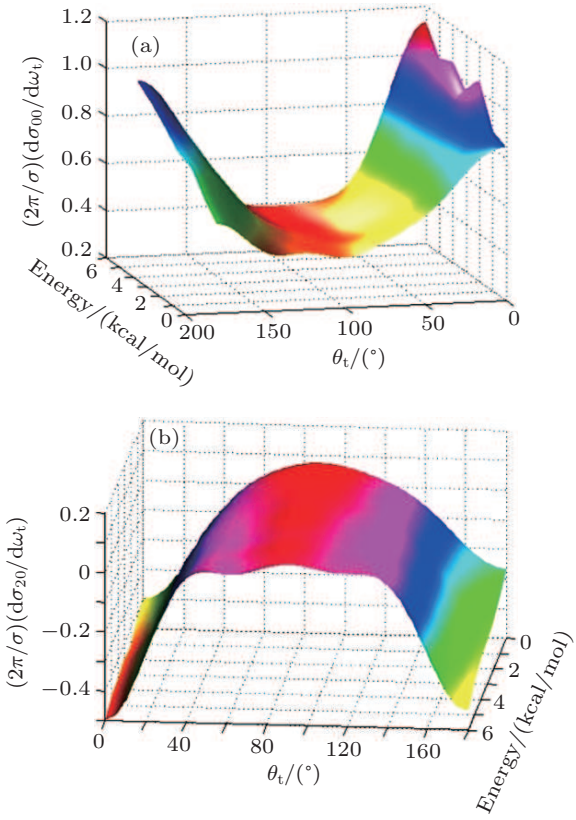


Fig. 2. (color online) Two PDDCSs of collision energies at $E_c=0$–6 kcal/mol with (a) $(k,q)=(0,0)$; (b) $(k,q)=(2,0)$.

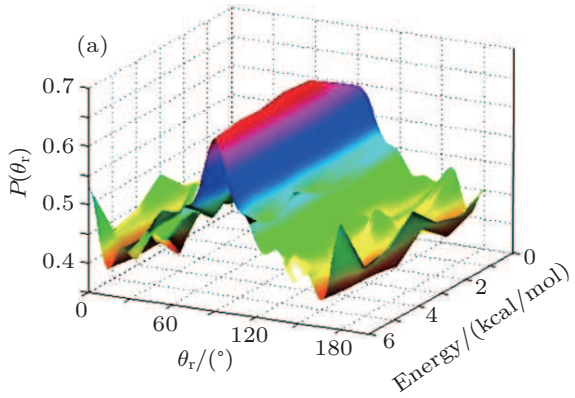


Fig. 3. (color online) Distributions of $P(\theta_r)$ reflecting $\boldsymbol{k}$–$\boldsymbol{j}'$ correlations at collision energies ranging from 0 kcal/mol to 6 kcal/mol.

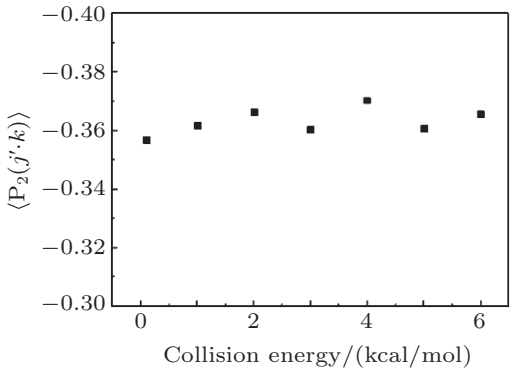


Fig. 4. Variation of rotational alignment parameter $\langle \mathrm{P}_2(j'\cdot k)\rangle$ with collision energy E_c in a range from 0 kcal/mol to 6 kcal/mol for the title reaction.

Figure 5 illustrates the dihedral angle distribution $P(\phi_r)$ which describes the $\boldsymbol{k}$–$\boldsymbol{k}'$–$\boldsymbol{j}'$ correlation. The computation values of collision energy E_c are in a range of 0 kcal/mol–6 kcal/mol from the inside to the outside. As seen from Fig. 5, the distributions of $P(\phi_r)$ are asymmetric with $\phi_r = 180°$ at all calculated collision energies, which reveals a strong polarization of the angular momentum. We can also obtain that there is no clear peak, but the average values are located in the vicinity of $\phi_r = 90°$ and $\phi_r = 270°$. Meanwhile, values at $\phi_r = 90°$ are stronger than those at $\phi_r = 270°$ which reflects the fact that the rotational angular momentum vector $\boldsymbol{j}'$ is oriented along the positive direction of the y axis. This phenomenon may be attributed to its light–heavy–heavy (LHH) mass combination that is similar to the result given by Meng *et al.*[39] The reagent orbital angular momentum $\boldsymbol{L}$ transfers into the product orbital alignment, and $\boldsymbol{j}'$ is independent of $\boldsymbol{L}$, which can be explained by the impulsive model for $A + BC \rightarrow AB + C$ reaction suggested by Han *et al.*[40–42] The angular momentum vector $\boldsymbol{j}'$ of the project is given by

$$j' = L\sin^2\beta + j\cos^2\beta + J_1 m_A/m_B, \tag{14}$$

$$\cos^2\beta = \frac{m_A \cdot m_C}{(m_A + m_B)(m_B + m_C)}, \tag{15}$$

$$J_1 = (\mu_{BC}R)^{1/2}(r_{AB} \times r_{CB}), \tag{16}$$

where L is the reagent orbital angular momentum, r_{AB} and r_{CB} are the unit vectors, R is the repulsive energy, and μ_{BC} is the reduced mass of reagent molecule BC. The term $L\sin^2\beta + j\cos^2\beta$ is symmetric. The term J_1 plays an important part in determining the rotational orientation. For the influence of the repulsive energy R, the term $J_1 m_A/m_B$ indicates a prioritized direction which leads to the left-handed HBr product rotation in the plane parallel to the $\boldsymbol{k}$–$\boldsymbol{k}'$ scattering plane.

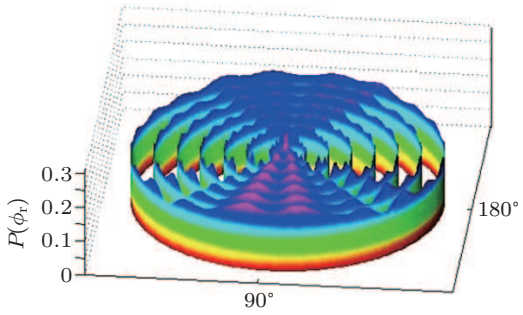


Fig. 5. (color online) Dihedral angle distribution of $P(\phi_r)$ with respect to the $\boldsymbol{k}$–k' plane, displayed in a reagent collision energy E_c (in a range of 0 kcal/mol–6 kcal/mol) from inside to outside.

In order to have an overall observation for the angular momentum polarization, the distributions of $P(\theta_r, \phi_r)$ with the effect of the collision energy are shown in Figs. 6(a)–6(c). For saving the space and without loss of generality, we only display the distributions with peaks and valleys at collision energy $E_c = 0$, 3, and 6 kcal/mol. As seen in Fig. 6, there are two main peaks at $(90°, 90°)$ and $(90°, 270°)$ which are consistent with the above-mentioned investigations. Meanwhile, it also implies that the HBr molecules are strongly polarized in the direction perpendicular to the scattering plane and generally rotate in the plane parallel to the scattering plane.

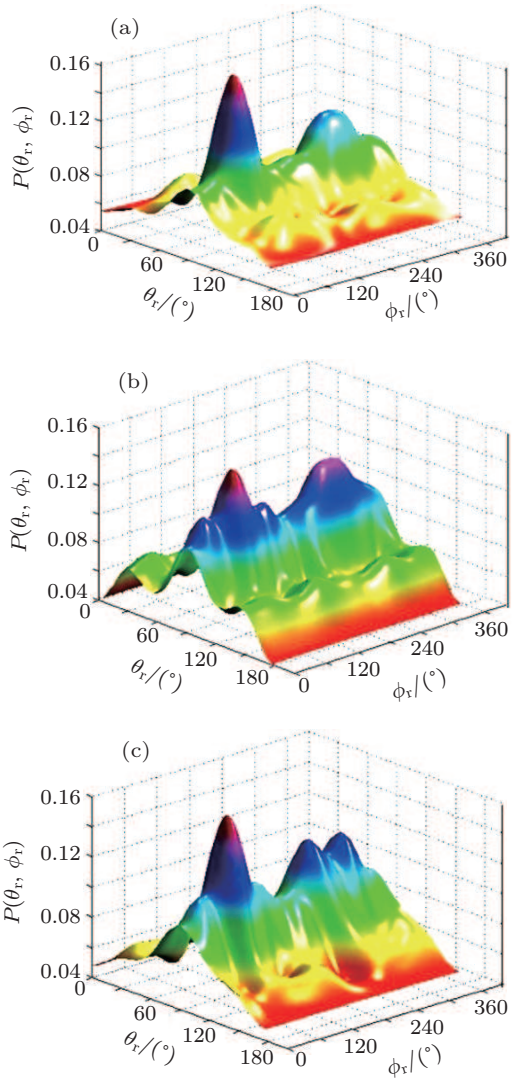


Fig. 6. (color online) Polar plots of the $P(\theta_r, \phi_r)$ distributions with peaks and valleys at different collision energies: $E_c = 0$ (a), 3 (b), and 6 (c).

4. Conclusions

Collision energy effect on the stereodynamics of $H + BrO \rightarrow O + HBr$ reaction is investigated on the ground state *ab initio* potential energy surface at E_c = 0kcal/mol–6 kcal/mol. In this paper, we calculate the polarization-dependent generalized differential cross section and the angular distributions of $P(\theta_r)$ and $P(\phi_r)$. Since there is a deep potential well on the PES, it leads to the formation of a long-lifetime intermediate complex which is indicated as the variation of the forward and backward scattering. As collision energy increases, the behavior of $PDDCS_{00}$ shows a rising strong scattering forward and backward trend, which means that the lifetime of the intermediate complex in the deep well

increases. The $PDDCS_{20}$ demonstrates that $\boldsymbol{j}'$ is strongly aligned in the direction perpendicular to $\boldsymbol{k}$. Distribution of $P(\theta_r)$ illustrates that the rotational angular momentum vector $\boldsymbol{j}'$ prefers aligning strongly along the direction perpendicular to the direction of $\boldsymbol{k}$. The $P(\phi_r)$ distribution shows an asymmetric behavior to the scattering plane and two peaks at $\phi_r = 90^\circ$ and $\phi_r = 270^\circ$ which indicates that $\boldsymbol{j}'$ is not only aligned but also oriented along the positive direction of the y axis, which can be explained by the impulsive model. The results of $P(\theta_r)$ and $P(\phi_r)$ are confirmed by the distributions of $P(\theta_r, \phi_r)$. In summary, the collision energy has relatively obvious effects on product polarization and angular distributions of the title reaction and also affects the intermediate complex formed in the deep well.

Acknowledgment

Many thanks to Prof. Han Ke-Li for providing the stereodynamics program. This article supported by High Performance Computing Center of Jilin University, China.

References

[1] Ruscic B and Berkowitz J 1994 *J. Chem. Phys.* **101** 7795
[2] Orlando J J and Burkholder J B 1995 *J. Phys. Chem.* **99** 1143
[3] Lee J J 1995 *J. Phys. Chem.* **99** 15074
[4] Spencer J E and Glass G P 1977 *Int. J. Chem. Kinet.* **9** 97
[5] Palmieri P, Puzzarini C and Tarroni R 1996 *Chem. Phys. Lett.* **256** 409
[6] Balucani N, Beneventi L, Casavecchia P, Volpi G G, Kruss E G and Sloan J J 1994 *Can. J. Chem.* **72** 888
[7] Wine P H, Wells J R and Ravishankara A R 1986 *J. Chem. Phys.* **84** 1349
[8] McRae G A and Cohen E A 1990 *J. Mol. Spectrosc.* **139** 369
[9] Orphal J, Kou Q, Tchana F K, Pirali O and Flaud J M 2003 *J. Mol. Spectrosc.* **221** 239
[10] Brouard M and Valance C 2001 *Phys. Chem. Chem. Phys.* **3** 3602
[11] Peterson K A 2000 *J. Chem. Phys.* **113** 4598
[12] Tang B Y, Tang Q K, Chen M D, Han K L and Zhang J Z H 2004 *J. Chem. Phys.* **120** 8537
[13] Zuo G P, Tang B Y and Han K L 2005 *Acta. Phys. Chim. Sin.* **21** 1022
[14] Zhang Y Y, Shi Y, Xie T X, Jin M X and Hu Z 2013 *Chin. Phys. B* **22** 083402
[15] Martínez T, Hernández M L, Avari J M, Laganà A, Aoiz F J, Menéndez M and Verdasco E 2000 *Phys. Chem. Chem. Phys.* **2** 589
[16] Zhao D, Zhang T Y and Chu T S 2010 *Can. J. Chem.* **88** 893
[17] Chu T S, Zhang H, Yuan S P, Fu A P, Si H Z, Tian F H and Duan Y B 2009 *J. Phys. Chem. A* **113** 3470
[18] Zhou S W, Wang Y H and Lu R F 2012 *Chem. Phys.* **402** 113
[19] Han B R, Zong F J, Wang C L, Ma W Y and Zhou J H 2010 *Chem. Phys.* **374** 94
[20] Chen M D, Tang B Y, Han K L and Lou N Q 2001 *Chem. Phys. Lett.* **337** 349
[21] Chen M D, Han K L and Lou N Q 2002 *Chem. Phys.* **283** 463
[22] Meng Q T, Zhao J, Xu Y and Yue D G 2009 *Chem. Phys.* **362** 65
[23] Ju L P, Han K L and Zhang J Z H 2009 *J. Comput. Chem.* **30** 305
[24] Ma J J, Chen M D, Cong S L and Han K L 2006 *Chem. Phys.* **327** 529
[25] Aoiz F J, Herrero V J and Sáez R V 1992 *J. Chem. Phys.* **97** 7423
[26] Zhao D, Chu T S and Hao C 2013 *Chin. Phys. B* **22** 063401
[27] Wang M L, Han K L, Zhan J P, Wu V W K, He G Z and Lou N Q 1997 *Chem. Phys. Lett.* **278** 307
[28] Chen M D, Han K L and Lou N Q 2002 *Chem. Phys.* **283** 463
[29] Han K L, He G Z and Lou N Q 1992 *Chin. J. Chem. Phys.* **96** 7865
[30] Han K L, He G Z and Lou N Q 1991 *Chem. Phys. Lett.* **178** 528
[31] Xie T X, Zhang Y, Zhao M Y and Han K L 2003 *Phys. Chem. Chem. Phys.* **5** 2034
[32] Yao C X and Zhao G J 2013 *Chin. Phys. B* **22** 083403
[33] Li W L, Wang M S, Yang C L, Liu W W, Sun C and Ren T Q 2007 *Chem. Phys.* **337** 93
[34] Aoiz F J, Brouard M and Enriquez P A 1996 *J. Chem. Phys.* **105** 4964
[35] Wang M L, Han K L and He G Z 1998 *J. Chem. Phys.* **109** 5446
[36] Wang L Z, Yang C L, Liang J J, Xiao J and Zhang Q G 2011 *Chin. J. Chem. Phys.* **24** 686
[37] Han K L, Zhang L, Xu D L, He G Z and Lou N Q 2001 *J. Phys. Chem. A* **105** 2956
[38] Liu Y F, Zhang W, Shi D H and Sun J F 2009 *Chin. Phys. B* **18** 4264
[39] Meng Q T, Zhao J, Xu Y and Yue D G 2009 *Chem. Phys.* **362** 65
[40] Han K L, He G Z and Lou N Q 1996 *J. Chem. Phys.* **105** 8699
[41] Han K L, Zhang L, Xu D L, He G Z and Lou N Q 2001 *J. Phys. Chem. A* **105** 2956
[42] Wang M L, Han K L and He G Z 1998 *J. Phys. Chem. A* **102** 10204